

Machine Learning for Survival Analysis: A New Approach

David Dooling^{1,✉}, Angela Kim^{1,‡}, Jennifer Webster^{1,✉}

1 Innovative Oncology Business Solutions, Albuquerque, NM, USA

✉These authors contributed equally to this work.

‡These authors also contributed equally to this work.

* ddooling@innovativeobs.com

Abstract

We have applied a little-known data transformation to subsets of the Surveillance, Epidemiology, and End Results (SEER) publically available data of the National Cancer Institute (NCI) to make it suitable input to standard machine learning classifiers. This transformation properly treats the right-censored data in the SEER data and the resulting Random Forest and Multi-Layer Perceptron models predict full survival curves. Treating the 6, 12, and 60 months points of the resulting survival curves as 3 binary classifiers, the 18 resulting classifiers have AUC values ranging from .765 to .885. Further evidence that the models have generalized well from the training data is provided by the extremely high levels of agreement between the random forest and neural network models predictions on the 6, 12, and 60 month binary classifiers.

Author Summary

Lorem ipsum dolor sit amet, consectetur adipiscing elit. Curabitur eget porta erat. Morbi consectetur est vel gravida pretium. Suspendisse ut dui eu ante cursus gravida non sed sem. Nullam sapien tellus, commodo id velit id, eleifend volutpat quam. Phasellus mauris velit, dapibus finibus elementum vel, pulvinar non tellus. Nunc pellentesque pretium diam, quis maximus dolor faucibus id. Nunc convallis sodales ante, ut ullamcorper est egestas vitae. Nam sit amet enim ultrices, ultrices elit pulvinar, volutpat risus.

Introduction

Opportunities are emerging in many industries today to develop and deploy services that cater to individual needs and preferences. Music afficianados can create their own radio stations tailored to their individual tastes from Pandora¹, bibliophiles can receive highly trustworthy book recommendations from goodreads.com², and Google will provide directions between any two points, giving options such as mode of transportation and as well as warnings of delays in realtime.³ These individualized services share many

¹Pandora Internet Radio - Listen to Free Music You'll Love, <http://www.pandora.com/> (accessed 27 Jan 2016)

²Share Book Recommendations With Your Friends, Join Book Clubs, Answer Trivia, <https://www.goodreads.com/> (accessed 27 Jan 2016)

³Google Maps, <https://goo.gl/1D7Jwf> (accessed 27 Jan 2016)

common features. In particular, they leverage large databases of aggregated information to learn and extract information relevant to individuals. Extracting actionable information from data is changing the fabric of modern business. A class of techniques that transforms data into actionable information goes by the name of Machine Learning [1]. Machine Learning has recently become a popular method to answer questions and solve problems that are too complex to solve via traditional methods.

The primary objective of this study is to show how machine learning methods can be trained with data in cancer registries to produce personalized survival prognosis curves, but the methods presented below can be applied to any type of survival data. Traditionally, cancer survival curves have been estimated using Kaplan-Meier methods [2]. Kaplan-Meier methodology also uses large datasets to make predictions, but the resulting information is not personal; the resulting curves are summaries for a population and not necessarily relevant or particularly accurate for any given individual. This property of Kaplan-Meier methods is exacerbated when dealing with heterogeneous populations. The methods described below also take full advantage of all relevant aggregate information, but are able to provide personalized survival curves relevant to individual subjects. This objective is in keeping with the recent movement in medicine known as Predictive, Preventive and Personalized Medicine (PPPM), which aims to leverage increasing amounts of health related data to maximize quality of care and to intelligently eliminate inefficient and unnecessary use of resources [3]. This capability of providing individualized survival curve prognosis is a direct result of the recent advances in computing power and machine learning algorithms, and similar methodology is becoming commonplace in many industries. These techniques are now infiltrating the healthcare industry, in spite of some of the data aggregation challenges posed by the Health Insurance Portability and Accountability Act (HIPPA) of 1996. This study makes use of a freely available data source that circumvents the restrictions imposed by HIPPA.

The Surveillance, Epidemiology, and End Results (SEER) Program of the National Cancer Institute (NCI) has been collecting data because intuitively researchers feel confident that this data will eventually allow researchers to detect information crucial to patients and providers including the relationships between the types of data collected (demographic as well as staging information, treatment and disease characteristics) and the survival outcomes. Though these relationships evade capture by traditional methods, it is possible to surface them with two machine learning techniques known as *Random Forests* and *Neural Networks*. As will be demonstrated in section , these two methods produce very similar results when applied to the SEER dataset, and are based on almost diametrically opposed learning philosophies, which lends confidence in the validity of the results.

The Surveillance, Epidemiology, and End Results (SEER) Program of the National Cancer Institute (NCI) is the most recognized authoritative source of information on cancer incidence and survival in the United States. SEER currently collects and publishes cancer incidence and survival data from population-based cancer registries covering approximately 28 percent of the US population.

Quoting directly from the SEER website [4]:

The SEER program registries routinely collect data on patient demographics, primary tumor site, tumor morphology and stage at diagnosis, first course of treatment, and follow-up for vital status. This program is the only comprehensive source of population-based information in the United States that includes stage of cancer at the time of diagnosis and patient survival data. The mortality data reported by SEER are provided by the National Center for Health Statistics. The population data used in calculating cancer rates is obtained periodically from the Census Bureau.

Updated annually and provided as a public service in print and electronic formats, SEER data are used by thousands of researchers, clinicians, public health officials, legislators, policymakers, community groups, and the public.

One characteristic of the SEER data that is shared by many datasets in the medical field goes by the name of "censored data." Observations are labeled censored when the survival time information is incomplete. The SEER data contains the number of months each patient survived, as well as an indicator variable showing whether or not the patient is still alive at the end of the data collection period. Methods to deal effectively with this kind of "right-censored data" include Kaplan-Meier curves and Cox Proportional Hazard models [2]. The Kaplan-Meier techniques only give estimates for cohorts of patients and are not applicable for predicting the survival curve for a single patient, and the Cox Proportional Hazard models require a fairly restrictive set of assumptions to be satisfied in order to yield reliable results.

Previous work applying machine learning methods to subsets of the SEER data include creative attempts to deal with the problems presented by "right-censored data." Shin et al. [5] use semi-supervised learning techniques to predict 5 year survival, essentially imputing values for SEER records where the survival months information is censored at a value less than 5 years. Zolbanin et al. [6] investigate the effects of comorbidities; i.e., patients with two different cancer diagnoses, but their treatment of the censored data underestimates the survival probabilities. All records representing patients who survived at least 60 months as well as all those who died earlier than 60 months were considered, but patients alive prior to 60 months but censored out of the study before 60 months were not included. This treatment biases the data and the predictions, leading to overly pessimistic survival probabilities predicted by the models.

Previous work applying machine learning methods based on decision trees to survival data in general have a long history, starting with Gordon et al. [7]. A summary of more recent developments concerning *survival trees* is provided by Bou-Hamad et al. [8]. These methods focus on altering the splitting criteria used in decision tree growth to account for the censoring, and use 1958 Kaplan-Meier methods at the resulting nodes for prediction purposes. These methods do not generalize to non-tree-based machine learning algorithms, though Ishwaran et al. have extended the methodology to *random survival forests*, ensembles of *survival trees* [9].

IOBS has applied a little-known technique to transform the SEER data to make it amenable to more powerful machine learning methods. Instead of modifying existing learning algorithms in drastic ways, we focus attention on the input data. This approach allows for different machine learning algorithms to use the same data with no modification. The essential idea is to recast the problem to an appropriate discrete classification problem instead of a regression problem (predicting survival months). Treating months after diagnosis as just another discrete feature, the SEER data (or any other right-censored data) can be transformed to make predictions for the hazard function (probability of dying in the next month, given that the patient has not yet died). The full survival function can then be derived from the hazard function.

This paper is organized as follows. We introduce the subsets of the SEER data used for this study, and present survival curves computed from traditional methods based on this data for the three cancer types *lung*, *breast*, and *colon*. We then present the essential methodology of this work, the data transformation that allows censored survival data to be used as input to existing machine learning classifiers. Then we present the details of the trained models, including some subtleties arising from the data transformation pertaining to the partition into training and test datasets. The method of deriving binary classifiers from the models' predictions for the survival curves is presented. In this paper, we have constructed binary classifiers corresponding to 6, 12, and 60 months, as these are standard metrics in cancer survival prognosis. Then follows

a discussion of the evaluation of the trained models. The performance metrics are the 18 AUC curves associated with the 6, 12, and 60 month survival binary classifiers for the two models associated with each cancer type. We also present additional evidence supporting validity of the predictions by computing the levels of agreement between the random forest and neural network models for each of the 18 binary classifiers and find striking agreement. Next we provide urls for 6 web applications that use the trained models to predict individual cancer survival prognosis curves. These apps are hosted on the popular Heroku website, and allow for exploration of the nonlinear relationships between the input features and resulting survival prognosis. It is exactly these kinds of tools that are the goal of Predictive, Preventive and Personalized Medicine. Finally, we present avenues for future research.

Materials and Methods

For this study we use the publically available 1973-2012 SEER incidence data files corresponding to colon, breast and lung cancer contained in the list below. SEER requires that researchers submit a request for the data, which includes an agreement form. Detailed documentation explaining the contents of both the incidence data files used in this study as well as a data dictionary for the 1973-2012 SEER incidence data files are available without the need to register or submit a data request [10].

- incidence\yr1973_2012.seer9\COLRECT.txt
- incidence\yr1973_2012.seer9\BREAST.txt
- incidence\yr1973_2012.seer9\RESPIR.txt
- incidence\yr1992_2012.sj_la_rg_ak\COLRECT.txt
- incidence\yr1992_2012.sj_la_rg_ak\BREAST.txt
- incidence\yr1992_2012.sj_la_rg_ak\RESPIR.txt
- incidence\yr2000_2012.ca_ky_lo_nj_ga\COLRECT.txt
- incidence\yr2000_2012.ca_ky_lo_nj_ga\BREAST.txt
- incidence\yr2000_2012.ca_ky_lo_nj_ga\RESPIR.txt
- incidence\yr2005_lo_2nd_half\COLRECT.txt
- incidence\yr2005_lo_2nd_half\BREAST.txt
- incidence\yr2005_lo_2nd_half\RESPIR.txt

Data preparation and preprocessing

A great deal of data munging is necessary before using these SEER incidence files as input into machine learning algorithms. A preprocessing step common to each of the three cancer types studied involves the SEER **STATE-COUNTY RECODE** variable. The **STATE-COUNTY RECODE** field is a state-county combination where the first two characters represent the state FIPS code and the last three digits represent the FIPS county code. The FIPS code is a five-digit Federal Information Processing Standard (FIPS) code which uniquely identifies counties and county equivalents in the United States, certain U.S. possessions, and certain freely associated states. This particular field illustrates an important characteristic of machine learning, that is, the difference between *categorical features* and *numeric features*. All input into a machine learning algorithm must be numeric, but real numbers carry with them the usually extremely useful property known as the well-ordering property. Machine learning algorithms use the well-ordering property of the real numbers to learn. But if one is tasked with encoding a categorical feature into suitable numeric format for machine learning, it is necessary to do so in a way that removes the well-ordering property [11].

As a simple example of how to correctly treat categorical variables in a machine learning context, consider the SEER variable **SEX**. This variable is encoded in the

Code	Description
1	Male
2	Female

Table 1. Encoding of gender in the SEER incidence files. These types of categorical variables need to be transformed via one-hot-encoding.

SEER raw data files with a numeric 1 for males and a numeric 2 for females as shown in Table (1). Values such as "Male" and "Female" encoded as numbers are dangerous because if not handled properly, they can generate bogus results [12]. Leaving the information for **SEX** as in Table (1) implies that Female is somehow greater than Male. This implied ordering affects the machine learning algorithms' convergence on a model. Simply encoding Male by 2 and Female by 1 would result in a completely different model, because of the now completely reversed ordering implied in the **SEX** variable. The proper way to transform the SEER **SEX** variable is to create two additional variables: **sex_Male** and **sex_Female**, and then to eliminate the variables **SEX** and **sex_Male** (keeping both of the variables **sex_Male** and **sex_Female** is a redundant representation). For example,

$$\begin{array}{|c|} \hline \text{Sex} \\ \hline 1 \\ \hline \end{array} \rightarrow \begin{array}{|c|c|} \hline \text{sex_Male} & \text{sex_Female} \\ \hline 1 & 0 \\ \hline \end{array} \rightarrow \begin{array}{|c|} \hline \text{sex_Female} \\ \hline 0 \\ \hline \end{array} \quad (1)$$

and

$$\begin{array}{|c|} \hline \text{Sex} \\ \hline 2 \\ \hline \end{array} \rightarrow \begin{array}{|c|c|} \hline \text{sex_Male} & \text{sex_Female} \\ \hline 0 & 1 \\ \hline \end{array} \rightarrow \begin{array}{|c|} \hline \text{sex_Female} \\ \hline 1 \\ \hline \end{array} \quad (2)$$

The procedure outlined in Equations (1, 2) is known as one-hot encoding and needs to be applied to all of the nominal categorical variables in the SEER data that we wish to include in our predictive models. In particular, in order to include the geographical information contained in the SEER categorical variable **STATE-COUNTY RECODE**, it becomes necessary to create a new feature variable for each of the distinct (state,county) pairs in the data. In the United States, there are approximately 3,000 counties. Clearly, transforming the **STATE-COUNTY RECODE** data representation into distinct (state,county) columns will explode the dataset to become wider than is optimal for machine learning. Adding extra columns to your dataset, making it wider, requires more data rows (making it taller) in order for machine learning algorithms to effectively learn [11]. Because one-hot coding **STATE-COUNTY RECODE** would cause such drastic shape changes in our data, we wish to avoid doing so. Fortunately, this variable, though given as a categorical variable, is actually a recode for three ordinal variables. There is an ordering among the (state,county) columns, namely longitude, latitude, and elevation. We can transform the data in **STATE-COUNTY RECODE** into three new numerical columns: **lat**, **lng**, and **elevation**.

For example, Table (2) shows how five entries of **STATE-COUNTY RECODE** corresponding to counties within New Mexico can be represented by the **elevation**, **lat**, and **lng** features.

It is a simple exercise to construct the full lookup table from the SEER **STATE-COUNTY RECODE** variable to the corresponding three values **elevation**, **lat**, and **lng**. We use the publically available datafile from the United States Census Bureau [13] to map the state FIPS and county FIPS codes to query strings like those in the **address** field in Table (2). It is then possible to programmatically query the

Table 2. Example of the transformation of STATE-COUNTY RECODE to elevation, lat, and lng.

STATE-COUNTY RECODE	address	elevation	lat	lng
35001	Bernalillo+county+NM	5207.579772	35.017785	-106.629130
35003	Catron+county+NM	8089.242628	34.151517	-108.427605
35005	Chaves+county+NM	3559.931671	33.475739	-104.472330
35006	Cibola+county+NM	6443.415570	35.094756	-107.858387
35007	Colfax+county+NM	6147.749089	36.579976	-104.472330

Google Maps Geocoding API for the latitude and longitude [14], and the Google Maps Elevation API for the corresponding elevation [15]. An added benefit of this shift from the single categorical variable `STATE-COUNTY RECODE` to the three continuous numerical variables `lat`, `lng`, and `elevation` is that input into the web applications described later are not restricted to the states and counties covered in the SEER registries; in fact, the input to the models can be any address you would enter into Google Maps and calls to the Google Maps Geocoding API and the Google Maps Elevation API provide the conversion from the address string to the input variables `lat`, `lng`, and `elevation`. The full lookup table analogous to Table (2) is available from a GitHub repository containing supplemental information for this study [16].

This study focused on three different cancer types, namely colorectal cancer, lung cancer, and breast cancer. In the SEER data, there are instances of subjects with multiple rows; whenever a subject, or patient, is diagnosed with a new tumor, an additional record is added. In this study, we restrict attention to the data corresponding to the first record of each subject; i.e., we wish to make models that predict survival prognosis based on the data available right after diagnosis. The full set of conditions defining the subsets of the SEER data used in this study follows below.

The four COLRECT.txt files were imported into a pandas DataFrame object. This data was then filtered according to the conditions in Table (3). The RESPIR.txt and BREAST.txt files were imported into separate dataframes in similar fashion and filtered according to the conditions in Table (4) and Table (5), respectively. The SEER variable `CS TUMOR SIZE` records the tumor size in millimeters if known. But if not known, `CS TUMOR SIZE` is given as '999', to indicate that the tumor size is "Unknown; size not stated; not stated in pateint record." In this study, we discard those records, as indicated in Tables (5, 3, 4).

Table 3. Filters applied to the Colon Cancer data.

Column	Filter
SEQUENCE NUMBER-CENTRAL	≠ "Unspecified"
AGE AT DIAGNOSIS	≠ "Unknown age"
BIRTHDATE-YEAR	≠ "Unknown year of birth"
YEAR OF DIAGNOSIS	≥ 2004
SURVIVAL MONTHS FLAG	= "1"
CS TUMOR SIZE EXT/EVAL	≠ ""
CS TUMOR SIZE	≠ 999
SEER RECORD NUMBER	= 1
PRIMARY SITE	= "LARGE INTESTINE, (EXCL. APPENDIX)"
SEQUENCE NUMBER-CENTRAL	= 0

Table 4. Filters applied to the Lung Cancer data.

Column	Filter
SEQUENCE NUMBER-CENTRAL	≠ "Unspecified"
AGE AT DIAGNOSIS	≠ "Unknown age"
BIRTHDATE-YEAR	≠ "Unknown year of birth"
YEAR OF DIAGNOSIS	≥ 2004
SURVIVAL MONTHS FLAG	= "1"
CS TUMOR SIZE EXT/EVAL	≠ ""
CS TUMOR SIZE	≠ 999
SEER RECORD NUMBER	= 1
PRIMARY SITE	= "LUNG & BRONCHUS"
SEQUENCE NUMBER-CENTRAL	= 0

Table 5. Filters applied to the Breast Cancer data.

Column	Filter
SEQUENCE NUMBER-CENTRAL	≠ "Unspecified"
AGE AT DIAGNOSIS	≠ "Unknown age"
BIRTHDATE-YEAR	≠ "Unknown year of birth"
YEAR OF DIAGNOSIS	≥ 2004
SURVIVAL MONTHS FLAG	= "1"
CS TUMOR SIZE EXT/EVAL	≠ " "
CS TUMOR SIZE	≠ 999
SEER RECORD NUMBER	= 1
SEQUENCE NUMBER-CENTRAL	= 0

The following categorical features were one-hot encoded for each of the three datasets:

221

222

- SEX ,
 - MARITAL STATUS AT DX ,
 - RACE/ETHNICITY ,
 - SPANISH/HISPANIC ORIGIN ,
 - GRADE ,
 - PRIMARY SITE ,
 - LATERALITY ,
 - SEER HISTORIC STAGE A ,
 - HISTOLOGY RECODE--BROAD GROUPINGS ,
 - MONTH OF DIAGNOSIS ,
 - VITAL STATUS RECODE ,
- 223
- 224
- 225
- 226
- 227
- 228
- 229
- 230
- 231
- 232
- 233

and the STATE-COUNTY RECODE variable was dropped and replaced with the elevation , lat , and lng variables for all three datasets as illustrated in Table (2).

234

235

Before applying machine learning models trained with these datasets, we review below the salient features of survival analysis and censored data. We then describe in detail a method that takes full advantage of all the data, including the right-censored

236

237

238

data, and which involves a simple and intuitive transformation, culminating in the full set of features and target variable listed in the back of this report.

Traditional Survival Analysis

Survival analysis pertains to data containing survival times, which are *intervals* between certain kinds of events, e.g.; cancer diagnosis date and expiry date. These intervals are often affected by a kind of "partial missingness" called *censoring*. Censored data must be analyzed in a special way to avoid biased estimates and bogus conclusions. Special methods have been developed long ago to analyze censored data properly.

With survival data, including the SEER data considered in this study, you may not know the exact time of death for some subjects. Some of the SEER subjects are still alive at the the time of the latest SEER data release. When the **VITAL STATUS RECODE** variable indicates that the subject is still alive, the **SURVIVAL MONTHS** variable is only a lower bound on the true number of survival months; this is called the *date of last contact* mode of censoring. You know that each subject either died on a certain date or was definitely alive up to some last-seen date (and you don't know how far beyond that date he or she may ultimately have lived). The latter situation is called a *censored* observation.

Statisticians have developed some traditional techniques to utilize the partial information contained in censored observations: the life-table method and the Kaplan-Meier method. Both of these methods make use of the partial information to provide unbiased estimates of the two fundamental concepts: - *hazard* and *survival*, both of which are functions of time:

- **The hazard rate** $\lambda(t)$ is the probability of dying in the next small interval of time, assuming that the subject is alive right now.
- **The survival rate** $S(t)$ is the probability of living for a certain amount of time after some starting point.

Incorrect treatment of survival data still seen in practice, and leading to biased results, includes simply excluding all subjects with a censored survival time from any survival analysis, and *imputing* (replacing) the censored (last-seen) date with some reasonable value. Both of these techniques destroy the partial information contained in the censored observations and nullify the validity of the resulting estimates for the hazard rate and survival rate [2].

In 1958, Edward L. Kaplan and Paul Meier collaborated to publish the seminal paper on how to estimate the hazard and survival rates for data containing censored observations [17]. The method is straightforward and for small datasets can be performed by hand. As an example, consider the survival data shown in Table (6). In the Kaplan-Meier calculation of the survival curve, the first step is to sort the subjects in Table (6) labeled 0 through 9 by *Survival Time* in ascending order. This process results in the first two columns (*Censored Status*, and *Survival Times*) in Table (7). The *At Risk* column decreases by one for each row; in every row a subject has either been censored out of the study or has died. The hazard rate is then computed for each value of *Survival Time* (necessarily a discrete function because the number of subjects is countable), by dividing the value in *Censored Status* by the value in *At Risk*. The hazard function is shown in the *Hazard Function* column in Table (7). It is then straightforward to calculate the survival function; 1 - hazard function represents the probability of not dying in the next interval of time, assuming that the subject has survived up until now and is represented by column *Prob of Surv*. The cumulative survival probability can then be obtained by successively multiplying all these individual time-slice probabilities together. In order to survive 2.4 years, first the subject has to

survive .5 years, then survive .75 years, 2.3 years and 2.4 years. The probability of surviving 2.4 years is then the product of these 3 probabilities and is given as .666 in Table(7) in the *Survival Function* column. The Kaplan-Meier survival estimate corresponding to the data given in Table (6) is shown in Table (7).

Table 6. Example data to illustate traditional Survival Analysis.

Survival Time (Years)	Censored Status
0	0.75
1	6.10
2	7.00
3	2.40
4	0.50
5	4.50
6	3.50
7	5.80
8	2.30
9	5.20

Table 7. Kaplan-Meier table corresponding to the example data in Table (6).

Censored Status	Survival Time	At Risk	Hazard Function	Prob of Surv	Survival Function
4	0	0.50	10	0.000000	1.000000
0	1	0.75	9	0.111111	0.888889
8	1	2.30	8	0.125000	0.875000
3	1	2.40	7	0.142857	0.857143
6	0	3.50	6	0.000000	1.000000
5	1	4.50	5	0.200000	0.800000
9	1	5.20	4	0.250000	0.750000
7	0	5.80	3	0.000000	1.000000
1	1	6.10	2	0.500000	0.500000
2	0	7.00	1	0.000000	1.000000

After the above one-hot encoding procedure, the new variable `vital.status_recode_Dead` indicates that the patient is deceased if this variable = 1, or else that the patient's record is right-censored if this variable = 0. `SURVIVAL MONTHS` and `vital.status_recode_Dead` are all that is needed to construct the Kaplan-Meier estimates for the SEER datasets. The Kaplan-Meier estimates of the survival curves for colon (Figure (1)), lung (Figure (3)), and breast cancer (Figure (2)) are constructed from the full population of cancer patients in the respective datasets. An unsatisfactory feature of these curves is that these estimates are based on populations and data with enough heterogeneity to make them not very meaningful to an indiviual. Patients with very disparate characteristics are given the same prognosis by these Kaplan-Meier survival curve estimates. Therefore it is desirable to find robust predictors for survival curves of individual subjects where the input is an individual record as opposed to a population. We present below the data transformation that allows for machine learning to be applied to censored data.

Transformation of Censored Data for Machine Learning

In this section we describe an inuitive way to transform right-censored data appropriately so that it may be used as input to machine learning algorithms that learn

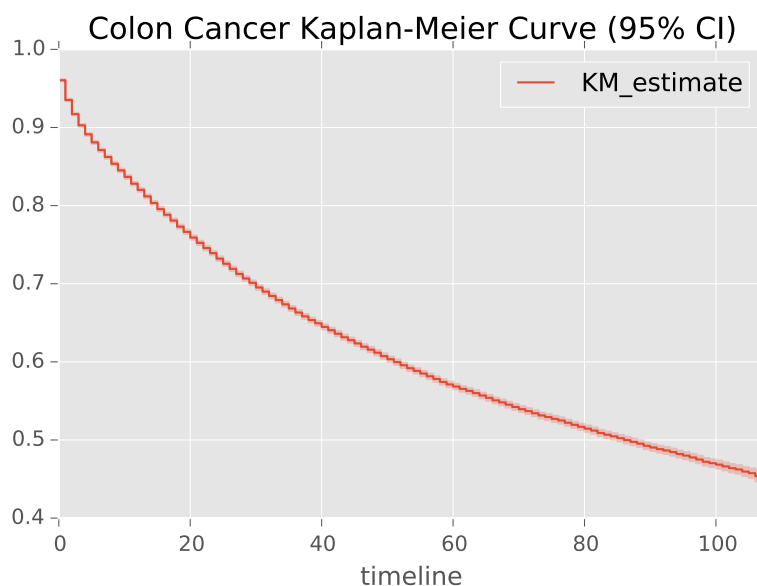


Figure 1. Traditional Kaplan-Meier estimate of the survival curve for all colon cancer patients. Fitted with 113072 observations, 71804 censored.

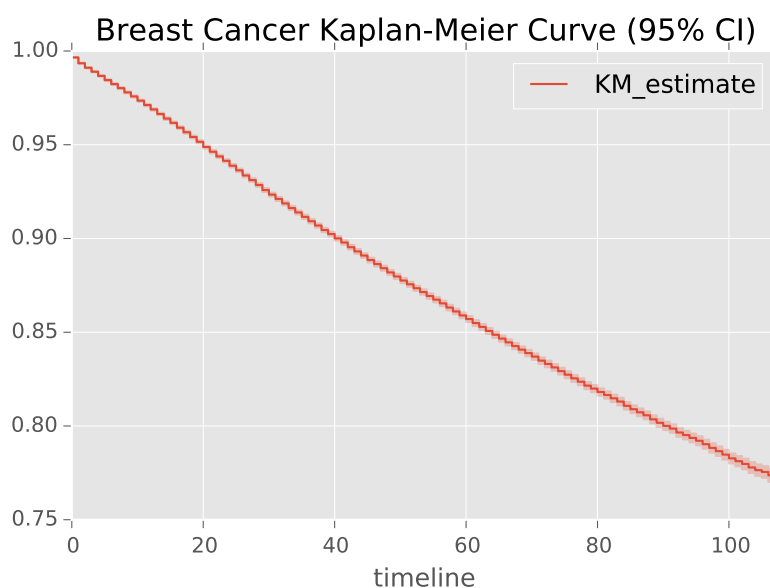


Figure 2. Traditional Kaplan-Meier estimate of the survival curve for all breast cancer patients. Fitted with 329949 observations, 292279 censored.

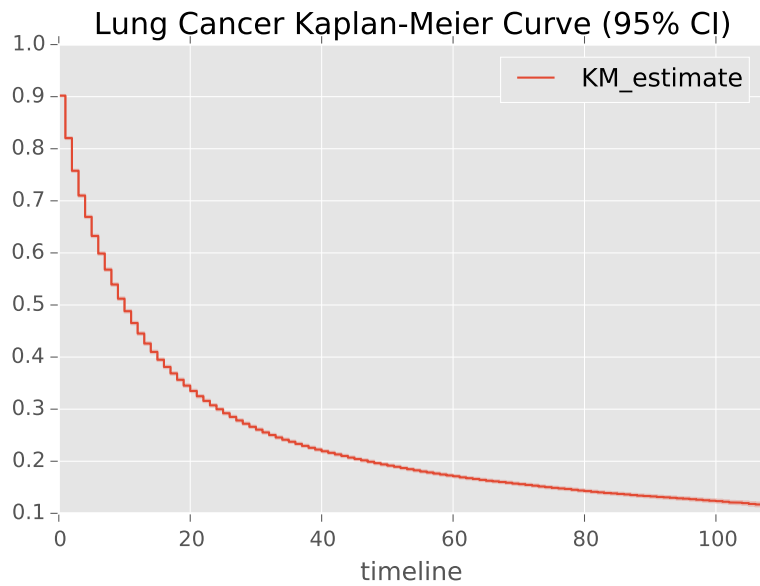


Figure 3. Traditional Kaplan-Meier estimate of the survival curve for all lung cancer patients. Fitted with 177089 observatins, 47409 censored.

the hazard fuction. The full details of this transformation, and a large inspiration for this study, can be flound in this blog post [18].

The overall philosophy of the Kaplan-Meier estimate of the survival curve for a population differs fundamentally from the methods described below and used in this study. The Kaplan-Meier estimate of the survival curve is given by

$$\hat{S}(t) = \prod_{t_i < t} \frac{n_i - d_i}{n_i} \quad (3)$$

where d_i are the number of death events at time t and n_t is the number of subjects at risk of death just prior to time t . Equation (3) uses the entire data set to arrive at an estimate of the entire population survival curve. In contrast, the method described below uses the entire data set to learn a model so as to predict hazard and survival curves from the data for as yet unseen individuals.

The key observation is to note that the hazard function can be directly learned via standard machine learning methods. It can be rewritten as

$$\lambda(\mathbf{X}, t) = P(Y = t | Y \geq t, \mathbf{X}), \quad (4)$$

the probability that, if someone has survived up until month t , they will die in that month. where \mathbf{X} represents all of the data for that particular record, and in our case Y represents the true, uncensored number of survival months of the patient. What is actually provided in the SEER data is the related variable SURVIVAL MONTHS T (how long each subject was in the study), and whether they exited by dying or being censored (D), VITAL STATUS RECODE . D is a Boolean variable, so $D = 1$ if $T = Y$, and $D = 0$ if $T < Y$.

It follows directly from equation 4 that

$$P(Y = t | \mathbf{X}) = \lambda(\mathbf{X}, t) \prod_{i=1}^{t-1} (1 - \lambda(\mathbf{X}, i)) \quad (5)$$

, which is the full probability distribution of dying at time Y [18]. The survival function is then readily derived from this distribution as

$$S(\mathbf{X}, t_k) = 1 - CDF(\mathbf{X}, t_k) \quad (6)$$

where $CDF(\mathbf{X}, t_k) = \sum_{k=1}^n P(Y = t_k | \mathbf{X})$ is the cumulative density function corresponding to the probability mass function in equation 5 [12].

Treating T as just another covariate is the key to the transformation. Each datapoint in the hidden classification problem is the combination of an \mathbf{X}_i in the original dataset plus some month t , and the classification problem is "did point \mathbf{X}_i die in month t ." We will call this new variable D_{it} (`newtarget`). We can transform our original data set into a new one, with one row for each month that each \mathbf{X}_i is in the sample; train a standard classifier on this new dataset with D_{it} as the target, and derive a survival model from the original dataset. Psuedocode for this transformation is found in section Pseudocode for the Data Transformation.

Explicit examples will help make this transformation clear. The untransformed datapoint represented Table (8) is transformed to the multiple records shown in Table (10). All uncensored data is transformed in this way. All censored data is similarly transformed. The untransformed datapoint represented Table (9) is transformed to the multiple records shown in Table (11).

Table 8. Example of four columns in an uncensored record in the untransformed dataset.

	cs_tumor_size	year_of_birth	survival_months	vital_status_recode_Death
newindex				
205	60	1951	3	1

Table 9. Example of four columns in a censored record in the untransformed dataset.

	cs_tumor_size	year_of_birth	survival_months	vital_status_recode_Death
newindex				
205	40	1950	3	0

Table 10. Example of four columns in an uncensored record in the transformed dataset.

	cs_tumor_size	year_of_birth	month	newtarget
newindex				
205	60	1951	0	0
205	60	1951	1	0
205	60	1951	2	0
205	60	1951	3	1

One obvious side effect of this transformation is that it explodes the length of the dataset. For this study, the original, untransformed colon cancer DataFrame has shape (113072, 103), and the total transformed colon cancer DataFrame has shape (4165251, 103). Similarly, the original, untransformed lung cancer DataFrame has shape (177089, 115), and the total transformed lung cancer DataFrame has shape (3079931, 115). The biggest explosion in dataset size occurred with the breast cancer data, which is a consequence of the relatively high survival rates in breast cancer. A subject who is censored with a recorded survival months of 48 will contribute an extra

Table 11. Example of four columns in a censored record in the transformed dataset.

	cs_tumor_size	year_of_birth	month	newtarget
newindex				
205	40	1950	0	0
205	40	1950	1	0
205	40	1950	2	0
205	40	1950	3	0

48 rows to the transformed dataset. The original, untransformed breast cancer DataFrame has shape (329949, 67), and the total transformed breast cancer DataFrame has shape (15085711, 67). Training machine learning algorithms on such large datasets, even after splitting into training and testing sets described below, require large RAM. All computations for this study were performed on a Dell XPS 8700 Desktop with 32GB of RAM.

Training and Test Partitions

After performing the data transformation adumbrated above, it is necessary to be mindful of how we partition the data into training and testing data. Each subject that was represented by a single row in the original untransformed dataset now potentially is represented by multiple rows in the transformed dataset, and care must be taken to ensure that all of the rows corresponding to a particular subject are either assigned exclusively to the training set or exclusive to the testing set. An additional characteristic of this transformed data that requires careful treatment involves balancing. The transformation results in many new records with the target variable `newtarget == 0`. The training and test sets must be chosen such that the ratio of the number of records with `newtarget == 0` to that of the number of records with `newtarget == 1` is the same in the training and test datasets. This ratio turns out to be ≈ 396 for the breast cancer data, ≈ 99 for the colon cancer data, and ≈ 22.75 for the lung cancer data. The shapes of the training and testing datasets for breast cancer used in this study are (14936862, 67) and (148849, 67), respectively. For lung cancer, the corresponding datasets have shapes (2988768, 115) and (91163, 115). Finally, for colon cancer the partition into training and test datasets of the transformed data have the shapes (3958008, 103) and (207243, 103). Multiple rows correspond to the same test patient in these datasets. The colon cancer test dataset represents 5654 distinct subjects; the breast cancer test dataset represents 3300 distinct subjects; and the lung test dataset contains data for 5313 distinct subjects.

The models described below are trained to learn the values of `newtarget`, which is a binary variable: a value of '0' indicating that the subject is still alive at the given month, while a value of '1' indicates that the patient died at that particular value of `months`. The random forests and neural networks described below are binary classifiers with the target `newtarget`. Fortunately, both the random forests and neural networks are capable of not only performing strict class prediction, i.e. predicting whether `newtarget` is '0' or '1', but are also able to predict the *probability* of `newtarget` being '0' or '1', and thus learning the hazard function.

Finally, we emphasize the crucial point that the features `survival_months` and `vital_status_recode_Dead` are dropped from both the training and testing data, and are replaced with the features `months` and `newtarget`, as illustrated in Tables (8, 9, 10, 11). The information of which subjects represent censored data

(`vital_status_recode_Dead == 0`) and which died is retained and recoverable through the `newindex` variable and is needed for proper evaluation of the performance metrics; when evaluating AUC curves for the 6, 12, and 60 month binary classifiers, we need to limit the test data to those subjects that we know definitively whether or not they survived 6, 12 or 60 months respectively. This requirement will necessitate the elimination of some of the censored data when computing some of the performance metrics. We introduce the two machine learning algorithms used in this study below, chosen because of their high performance in machine learning competitions and their complementary methods, so that their mutual agreement shown below on the test datasets can be taken as indication that they are actually learning useful information.

Random Forests are made up of an ensemble of independent **Decision trees** that are purposefully exposed to only subsets of the data. The general philosophy is presented in the popular science book "The Wisdom of Crowds" [19]. The idea is that a large number of independent non-expert opinions converge on the correct answer when averaged. The success of this philosophy of prediction was startlingly shown by the success of the political and world event predictions made by the prediction market site Intrade, before its forced closure by the Commodity Futures Trading Commission [20]. The other class of methods used by IOBS to develop predictive models are called neural networks, and are modelled on how the human brain learns high level concepts from lower level ones. As opposed to the crowd-based wisdom of a random forest, a neural network is analogous to a seasoned expert. A Neural network learns from repeated exposure to the training data and improves its predictions with each pass over the data. The general philosophy is similar to that represented by the well-known maxim that it takes 10,000 hours to become an expert in any given field [21].

Prediction Models

With the datasets transformed as described above, we are now able to use them to train and evaluate machine learning classifiers. The classifier models described in this section are learning the hazard function: given all of the data given in the Supporting Information section for each cancer type and includes the field `months` (the months after diagnosis), the models predict the target variable `newtarget`, which is a binary class label equal to 1 if the subject died in that month and 0 otherwise. Fortunately, both random forests and neural networks are capable of not only performing strict class prediction, i.e. predicting whether `newtarget` is 0 or 1, but are also able to predict the *probability* of `newtarget` being 0 or 1, and thus learning the hazard function. The models learn $\lambda(\mathbf{X}, \text{months})$. This prediction task should not be confused with the regression problem of trying to predict precisely in what month a patient will die.

The hazard functions thus learned and predicted are intermediary products; what we are really pursuing are the survival functions for each patient that are derived from the predicted hazard functions. From the resulting hazard functions for each unique patient, we can construct the resulting survival functions as presented in section () and Equation (??) and explicitly given in python code in the notebooks at the github repository containing supplemental material for this study [16]. For each subject i , all input data minus `months` and `newtarget` is represented by \mathbf{X}_i . After the classifier models have trained with target `newtarget` on the (very large) training set, each subject's survival function is computed in the corresponding (much smaller) test set. These functions are computed by using the model to predict $\lambda(\mathbf{X}_i, t_j)$ for j running from 0 to 107 months, and \mathbf{X}_i corresponds to the single row corresponding to subject i in the original untransformed dataset. 107 months was the maximum value of survival months in all three of the cancer datasets, and is a consequence of the data subsets

chosen for this study.

Decision Trees and Random Forests *Decision tree* classifiers are attractive models because they can be interpreted easily. Like the name decision tree suggests, we can think of this model as breaking down our data by making decisions based on asking a series of questions. Based on the features in our training set, the decision tree model learns a series of questions to infer the class labels of the samples.

Random forests have gained huge popularity in applications of machine learning during the last decade due to their good classification performance, scalability, and ease of use. Intuitively, a random forest can be considered as an *ensemble of decision trees*. The idea behind ensemble learning is to combine *weak learners* to build a more robust model, a *strong learner*, that has a better generalization error and is less susceptible to overfitting.

The goal behind *ensemble methods* is to combine different classifiers into a meta-classifier that has a better generalization performance than each individual classifier alone. For example, assuming that we collected predictions from 10 experts, ensemble methods would allow us to strategically combine these predictions by the 10 experts to come up with a prediction that is more accurate and robust than the predictions by each individual expert. The individual decision trees that make an ensemble are called base learners, and as long as the error rate of each base learner is less than .50, the combined random forest will benefit from the affects of combining predictions to achieve a far greater accuracy.

Figure (4) illustrates the power of ensemble methods; the Figure illustrates how the ensemble error rate is much lower than the Base learner error rate, as long as the Base learner error rate is less than 0.5. The Figure illustrates this effect for an ensemble of 500 base learners.

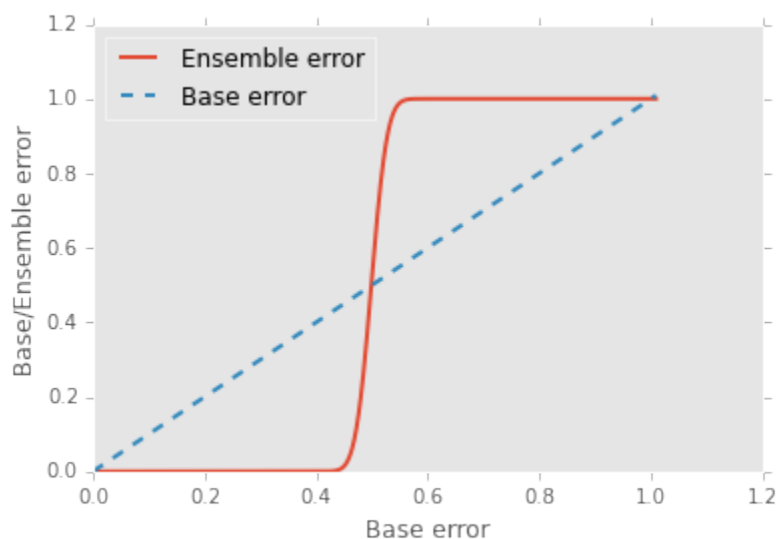


Figure 4. Illustration of ensemble methods showing how a collection of base learners with poor accuracy can combine to produce an accurate ensemble learner.

A big advantage of random forests is that honing in on suitable hyperparameter values (the number of trees in the forest, the depth of each decision tree, the specific measure of information gain used to choose the node splitting, etc) is not very difficult. The ensemble method is robust to noise from the individual decision trees, which helps to prevent overfitting (memorizing the training dataset targets instead of generalizing

from learned rules to perform successfully on unseen data). The only parameter that has a clearly noticeable effect on performance is the number of trees to include in the forest; in general, the more trees the better the performance, but there is a price to pay in terms of computational cost. The number of trees for the forests trained in this study was relatively small, 20 trees for breast cancer and 25 for both the lung and colon cancer models.

IOBS has chosen to use the Python scikit-learn implementation of the Random Forest machine learning classifier [22]. Random Forests are frequent winners of the Kaggle machine learning competitions [23]. The model parameters for each cancer type are given in sections (Lung Random Forest Model Hyperparameters, Colon Random Forest Model Hyperparameters, Breast Random Forest Model Hyperparameters).

Multi-Layer Perceptron Neural Networks Neural networks are a biologically-inspired programming paradigm that enable computers to learn from observational data [24]. Deep learning can be understood as a set of algorithms that were developed to train artificial neural networks with many layers most efficiently. Neural networks are a hot topic not only in academic research, but also in big technology companies such as Facebook, Microsoft, and Google who invest heavily in artificial neural networks and deep learning research. As of today, complex neural networks powered by deep learning algorithms are considered as state-of-the-art when it comes to complex problem solving such as image and voice recognition. In addition, the pharmaceutical industry recently started to use deep learning techniques for drug discovery and toxicity prediction, and research has shown that these novel techniques substantially exceed the performance of traditional methods for virtual screening [25].

IOBS has chosen to use the Multi-Layer Perceptron Neural Network (MLP neural network) implementation Keras developed at MIT. Keras was initially developed as part of the research effort of project ONEIROS (Open-ended Neuro-Electronic Intelligent Robot Operating System) [26]. Keras is a minimalist, highly modular neural networks library, written in Python and capable of running on top of either TensorFlow or Theano. The model architecture for each cancer type are given in sections (Breast Neural Network Model Architecture, Colon Cancer Neural Network Model Architecture, Lung Cancer Neural Network Model Architecture). Training a neural network and choosing an appropriate architecture is as much art as science [24], and the search for a good neural network architecture for the lung cancer case was more demanding than for the breast and colon cases. The presence of both non-small cell lung cancer (NSCLC) and small cell lung cancer (SCLC) in the SEER data may be the source of this need for more iterations and trials of different architectures when training the lung cancer neural network models.

Results

In order to evaluate the performance of the models, we first construct three binary classifiers corresponding to whether or not a subject survived 6, 12, or 60 months after diagnosis. This is done by iterating over all distinct patient indices in the test set, predicting the full survival function, and capturing the values corresponding to 6, 12, and 60 months. If the survival function evaluated at 6 months is greater than or equal to .5 for a given subject, then the 6 months binary classifier predicts that that subject will be alive 6 months after diagnosis. Similarly, if the survival function evaluated at 60 months is less than .5, then the 12 months binary classifier predicts that that subject will be dead 12 months after diagnosis. Figure (5) illustrates the method; in this case the 6-month and 12-month classifiers predict survival, while the 60-month classifier predicts expiry.

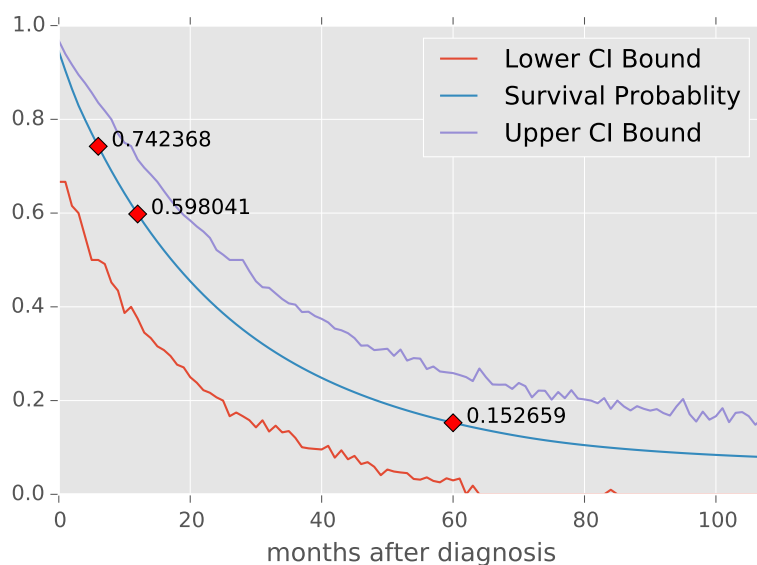


Figure 5. Example of the construction of the binary classifiers for 6, 12, and 60 months survival. A subject's hazard curve $\lambda(\mathbf{X}, t)$ is predicted by the model for times out to 107 months. The survival curve is then readily computed as in Equation (6). For this example, the 6-month and 12-month classifiers predict survival, while the 60-month classifier predicts expiry.

Because of censoring it is necessary to apply some Boolean filters to the data in order to correctly assess the resulting classifiers. To construct AUC curves for the 6 month classifier, we restrict ourselves to considering subjects in the test data where either of the following mutually exclusive conditions holds:

- `survival_months >= 6 AND vital_status_recode == 0`
- `vital_status_recode == 1`

That is, we restrict ourselves to subsets of the data where we know for certain whether or not the subject survived at least 6 months. Similarly for the 12 and 60 months survival classifiers.

Survival Curve Error Estimates The standard calculation of confidence intervals used in the Kaplan-Meier estimates of survival curves does not apply for these personal predictions. The following bootstrap method was used to calculate the upper and lower bounds corresponding to 95% confidence intervals. From equation 6, we can obtain the cumulative distribution function (CDF) associated with each individual survival curve. We then sample from this CDF in a way that reflects the underlying data used to produce the model. The training data used to create the model has an underlying distribution of survival months. In the transformed training dataset, each subject contributes as many rows as the number of survival months plus one (patients with zero survival months still represent one row of the training data). A subject that survived 50 months contributes 51 "points" to the training of the model. If all patients lived out to 107 months, the model would contain less uncertainty. This observation leads to the following algorithm for determining the error estimates to the predicted survival curves:

- compute the CDF associated with the survival curve

- use the underlying training data CDF of survival months to choose the number of points to draw from the survival curve CDF, and compute a new survival curve
- Repeat the previous step 10,000 times and collect the curves into a list. Changing the number of curves affects how smooth the upper and lower bounds are, but does not affect the interval size between for each month.
- extract for each month from the list of curves the .975 and .025 percentiles to record the values for the upper and lower curves

The process is somewhat analogous to the following hypothetical situation. Imagine a patient going to an expert, and the expert after collecting data on the patient and keeping records predicts the central, single survival curve. The patient then seeks multiple "second opinions." These second opinions are generated not from independent examinations of the patient, but by outside experts sampling from the data already collected by the expert initially consulted. Then the predictions of 95% of these 10,000 experts all fall within the band determined by the upper and lower curves.

Performance Metrics

The AUC scores for each of the 18 different binary classifiers are listed in Table (12). We emphasize the above-mentioned discussion concerning the correct treatment of the censored test data when evaluating performance metrics. Namely, when computing the AUC for the 12 month survival curve classifiers, we restrict the test data subjects to those that in the untransformed data set that satisfy either of the following mutually exclusive conditions:

- `survival_months >= 12 AND vital_status_recode == 0`
- `vital_status_recode == 1`

We limit evaluation data to subsets of the data where we know for certain whether or not the subject survived at least 12 months. Similar considerations apply to the 12 and 60 months AUC calculations. The lowest AUC in Table 12 is .765, corresponding to the lung neural network model predictions for 6 months survival, while the highest AUC in Table 12 is .885, corresponding to the breast random forest model predictions for 12 months survival.

Table 12. AUC values for the Random Forest and Neural Networks model binary classifiers derived from the full survival curve predictions; see text for details. The number of subjects that were used in the calculation of a given AUC score are given in parenthesis after the score.

Model	6 Months AUC	12 Months AUC	60 Months AUC
Breast RF	.846 (3035)	.885 (2797)	.844 (1392)
Breast NN	.855 (3035)	.867 (2797)	.836 (1392)
Colon RF	.804 (5281)	.806 (5003)	.828 (3232)
Colon NN	.797 (5281)	.804 (5003)	.841 (3232)
Lung RF	.772 (5019)	.796 (4860)	.874 (4143)
Lung NN	.765 (5019)	.796 (4860)	.875 (4143)

Model Agreement

An additional means of validating the predictions of these models is by comparing their predictions to each other for the same set of input data. Table 13 shows the strong agreement between the random forest and neural network classifiers for each cancer

type. Python code showing how the values in Table 13 are computed is available in the files `NewPatientBreastCF.html` , `NewPatientColonCF.html` , and `NewPatientLung.html` in the GitHub repository containing supplemental material for this study [16]. Table 13 is computed as follows. For each cancer type (breast,colon, and lung), do the following:

- use the corresponding Random Forest and Neural Network models to compute the survival curves for all of the test subjects
- extract the values of the survival curve evaluted for 6, 12, and 60 months for both models
- if both models predict less than .5 or both models predict greater than or equal to .5, that counts as agreement
- otherwise, the models disagree

The high level of agreement between two models lends confidence to the notion that they have both learned from the training data and are generalizing well. Figures (7, 6, 8) show box plots of the value of the random forest prediction subtracted from the neural network prediction. We emphasize that when evaluating the model agreement, we put no restrictions on the distinct subjects in the respective test datasets; we are confronting the models against each other, not some known ground truth as in the AUC performance metric calculations. The number of distinct subjects in all three of the colon cancer survival binary classifiers (6, 12, and 60 month survival) was 5654; for lung cancer the number of subjects entering into the calculation of Table (13) was 5313; and for breast cancer it was 3300.

Table 13. Percentage agreement for the Random Forest and Neural Network classifiers for 6, 12, and 60 month survival predictions on the test data for each cancer type.

Cancer Type	% agreement 6 months	% agreement 12 months	% agreement 60 months
Colon	.981	.971	.915
Breast	.994	.984	.938
Lung	.861	.883	.900

Survival Curve Prediction Apps

The six models described in section Prediction Models, namely the random forest and MLP neural network models for each of the three cancer types considered in this study, have their full hyperparameter and architecture presented in section Supporting Information. Python code for all six model training and evaluation is available at the githib respository containing supplemental material for this study [16].

LOREM and IPSUM Nunc blandit a tortor.

Maecenas convallis mauris sit amet sem ultrices gravida. Etiam eget sapien nibh. Sed ac ipsum eget enim egestas ullamcorper nec euismod ligula. Curabitur fringilla pulvinar lectus consectetur pellentesque. Quisque augue sem, tincidunt sit amet feugiat eget, ullamcorper sed velit. Sed non aliquet felis. Lorem ipsum dolor sit amet, consectetur adipiscing elit. Mauris commodo justo ac dui pretium imperdiet. Sed suscipit iaculis mi at feugiat.

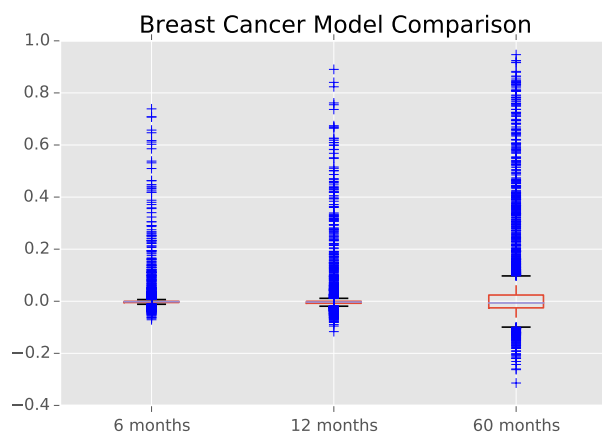


Figure 6. Box plots showing the distributions of the signed difference between the MLP model's prediction for the probability of surviving 6 months and the Random Forest model's prediction of the same quantity for breast cancer. The plot shows the same quantity for the 12 and 60 months classifiers. It is apparent from the figures that the outliers are due to the neural network models predicting higher survival probabilities than the random forest for some few cases. These differences were evaluated for the 3300 test patients in the breast cancer data.

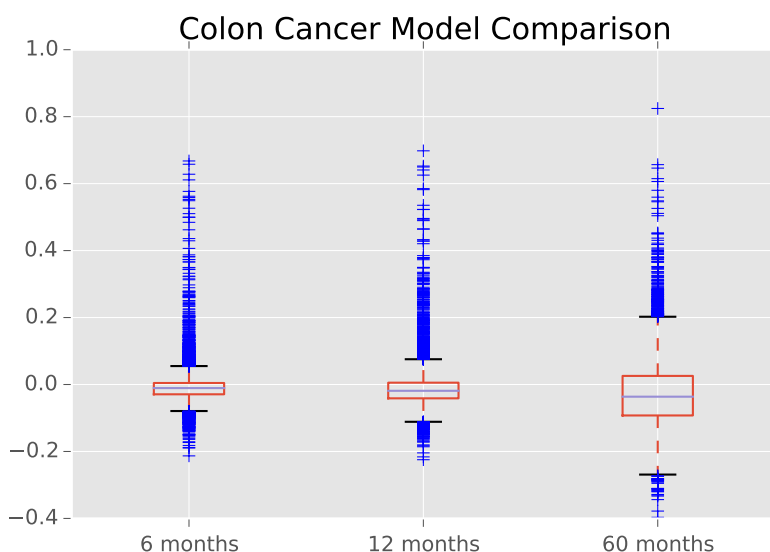


Figure 7. Box plots showing the distributions of the signed difference between the MLP model's prediction for the probability of surviving 6 months and the Random Forest model's prediction of the same quantity for colon cancer. The plot shows the same quantity for the 12 and 60 months classifiers. It is apparent from the figures that the outliers are due to the neural network models predicting higher survival probabilities than the random forest for some few cases. These differences were evaluated for the 5654 test patients in the colon cancer data.

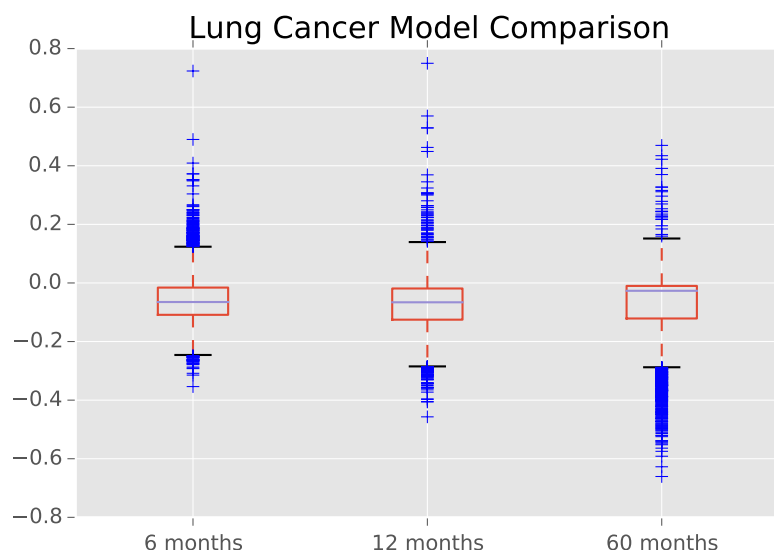


Figure 8. Box plots showing the distributions of the signed difference between the MLP model’s prediction for the probability of surviving 6 months and the Random Forest model’s prediction of the same quantity for lung cancer. The plot shows the same quantity for the 12 and 60 months classifiers. These differences were evaluated for the 5313 test patients in the lung cancer data. The Interquartile Ranges for lung cancer are visibly larger than those for breast cancer and colon cancer shown in fig 6 and fig 7.

Sed ac quam id nisi malesuada congue.

Nulla mi mi, venenatis sed ipsum varius, volutpat euismod diam. Proin rutrum vel massa non gravida. Quisque tempor sem et dignissim rutrum. Lorem ipsum dolor sit amet, consectetur adipiscing elit. Morbi at justo vitae nulla elementum commodo eu id massa. In vitae diam ac augue semper tincidunt eu ut eros. Fusce fringilla erat porttitor lectus cursus, vel sagittis arcu lobortis. Aliquam in enim semper, aliquam massa id, cursus neque. Praesent faucibus semper libero.

Subsection 1

Nulla mi mi, venenatis sed ipsum varius, volutpat euismod diam. Proin rutrum vel massa non gravida. Quisque tempor sem et dignissim rutrum. Lorem ipsum dolor sit amet, consectetur adipiscing elit. Morbi at justo vitae nulla elementum commodo eu id massa. In vitae diam ac augue semper tincidunt eu ut eros. Fusce fringilla erat porttitor lectus cursus, vel sagittis arcu lobortis. Aliquam in enim semper, aliquam massa id, cursus neque. Praesent faucibus semper libero.

Subsection 2

3rd Level Heading. Nulla mi mi, venenatis sed ipsum varius, volutpat euismod diam. Proin rutrum vel massa non gravida. Quisque tempor sem et dignissim rutrum. Lorem ipsum dolor sit amet, consectetur adipiscing elit. Morbi at justo vitae nulla elementum commodo eu id massa. In vitae diam ac augue semper tincidunt eu ut eros. Fusce fringilla erat porttitor lectus cursus, vel sagittis arcu lobortis. Aliquam in enim semper, aliquam massa id, cursus neque. Praesent faucibus semper libero.

Discussion

Nulla mi mi, venenatis sed ipsum varius, Table ?? volutpat euismod diam. Proin rutrum vel massa non gravida. Quisque tempor sem et dignissim rutrum. Lorem ipsum dolor sit amet, consectetur adipiscing elit. Morbi at justo vitae nulla elementum commodo eu id massa. In vitae diam ac augue semper tincidunt eu ut eros. Fusce fringilla erat porttitor lectus cursus, vel sagittis arcu lobortis. Aliquam in enim semper, aliquam massa id, cursus neque. Praesent faucibus semper libero.

LOREM and IPSUM Nunc blandit a tortor.

CO₂ Maecenas convallis mauris sit amet sem ultrices gravida. Etiam eget sapien nibh. Sed ac ipsum eget enim egestas ullamcorper nec euismod ligula. Curabitur fringilla pulvinar lectus consectetur pellentesque. Quisque augue sem, tincidunt sit amet feugiat eget, ullamcorper sed velit.

Sed non aliquet felis. Lorem ipsum dolor sit amet, consectetur adipiscing elit. Mauris commodo justo ac dui pretium imperdiet. Sed suscipit iaculis mi at feugiat. Ut neque ipsum, luctus id lacus ut, laoreet scelerisque urna. Phasellus venenatis, tortor nec vestibulum mattis, massa tortor interdum felis, nec pellentesque metus tortor nec nisl. Ut ornare mauris tellus, vel dapibus arcu suscipit sed. Nam condimentum sem eget mollis euismod. Nullam dui urna, gravida venenatis dui et, tincidunt sodales ex. Nunc est dui, sodales sed mauris nec, auctor sagittis leo. Aliquam tincidunt, ex in facilisis elementum, libero lectus luctus est, non vulputate nisl augue at dolor. For more information, see S1 Text.

Supporting Information

Colon Cancer Feature Selection

The feature set used as input into both the Random Forest and Neural Network models, after the transformation described in section Transformation of Censored Data for Machine Learning is given below and also available in full detail in the file `NewPatientColonML.html`.

- `cs_tumor_size`
- `elevation`
- `grade_cell` type not determined
- `grade_moderately` differentiated
- `grade_poorly` differentiated
- `grade_undifferentiated`; anaplastic
- `grade_well` differentiated
- `histology_recode_broad_groupings_acinar` cell neoplasms
- `histology_recode_broad_groupings_adenomas` and adenocarcinomas
- `histology_recode_broad_groupings_blood_vessel` tumors
- `histology_recode_broad_groupings_complex` epithelial neoplasms
- `histology_recode_broad_groupings_complex_mixed` and stromal neoplasms
- `histology_recode_broad_groupings_cystic`, mucinous and serous neoplasms
- `histology_recode_broad_groupings_ductal` and lobular neoplasms
- `histology_recode_broad_groupings_epithelial` neoplasms, NOS
- `histology_recode_broad_groupings_fibromatous` neoplasms
- `histology_recode_broad_groupings_germ_cell` neoplasms
- `histology_recode_broad_groupings_lipomatous` neoplasms
- `histology_recode_broad_groupings_miscellaneous` bone tumors

• histology_recode_broad_groupings_myomatous neoplasms	679
• histology_recode_broad_groupings_neuroepitheliomatous neoplasms	680
• histology_recode_broad_groupings_nevi and melanomas	681
• histology_recode_broad_groupings_paragangliomas and glumus tumors	682
• histology_recode_broad_groupings_soft tissue tumors and sarcomas, NOS	683
• histology_recode_broad_groupings_squamous cell neoplasms	684
• histology_recode_broad_groupings_synovial-like neoplasms	685
• histology_recode_broad_groupings_transistional cell papillomas and carcinomas	686
• histology_recode_broad_groupings_unspecified neoplasms	687
• lat	688
• laterality_Left: origin of primary	689
• laterality_Not a paired site	690
• laterality_Only one side involved, right or left origin unspecified	691
• laterality_Paired site, but no information concerning laterality; midline tumor	692
• laterality_Right: origin of primary	693
• lng	694
• marital_status_at_dx_Divorced	695
• marital_status_at_dx_Married (including common law)	696
• marital_status_at_dx_Separated	697
• marital_status_at_dx_Single (never married)	698
• marital_status_at_dx_Unknown	699
• marital_status_at_dx_Unmarried or domestic partner	700
• marital_status_at_dx_Widowed	701
• month_of_diagnosis_Apr	702
• month_of_diagnosis_Aug	703
• month_of_diagnosis_Dec	704
• month_of_diagnosis_Feb	705
• month_of_diagnosis_Jan	706
• month_of_diagnosis_Jul	707
• month_of_diagnosis_Jun	708
• month_of_diagnosis_Mar	709
• month_of_diagnosis_May	710
• month_of_diagnosis_Nov	711
• month_of_diagnosis_Oct	712
• month_of_diagnosis_Sep	713
• number_of primaries	714
• race_ethnicity_Amerian Indian, Aleutian, Alaskan Native or Eskimo	715
• race_ethnicity_Asian Indian	716
• race_ethnicity_Asian Indian or Pakistani	717
• race_ethnicity_Black	718
• race_ethnicity_Chinese	719
• race_ethnicity_Fiji Islander	720
• race_ethnicity_Filipino	721
• race_ethnicity_Guamanian	722
• race_ethnicity_Hawaiian	723
• race_ethnicity_Hmong	724
• race_ethnicity_Japanese	725
• race_ethnicity_Kampuchean	726
• race_ethnicity_Korean	727
• race_ethnicity_Laotian	728
• race_ethnicity_Melanesian	729
• race_ethnicity_Micronesian	730

- `race_ethnicity_New Guinean` 731
- `race_ethnicity_Other` 732
- `race_ethnicity_Other Asian` 733
- `race_ethnicity_Pacific Islander` 734
- `race_ethnicity_Pakistani` 735
- `race_ethnicity_Polynesian` 736
- `race_ethnicity_Samoan` 737
- `race_ethnicity_Thai` 738
- `race_ethnicity_Tongan` 739
- `race_ethnicity_Unknown` 740
- `race_ethnicity_Vietnamese` 741
- `race_ethnicity_White` 742
- `seer_historic_stage_a_Distant` 743
- `seer_historic_stage_a_In situ` 744
- `seer_historic_stage_a_Localized` 745
- `seer_historic_stage_a_Regional` 746
- `seer_historic_stage_a_Unstaged` 747
- `sex_Female` 748
- `spanish_hispanic_origin_Cuban` 749
- `spanish_hispanic_origin_Dominican Republic` 750
- `spanish_hispanic_origin_Mexican` 751
- `spanish_hispanic_origin_Non-Spanish/Non-hispanic` 752
- `spanish_hispanic_origin.Other specified Spanish/Hispanic origin (excludes Dominican Repuclic)` 753
- `spanish_hispanic_origin.Puerto Rican` 754
- `spanish_hispanic_origin.South or Central American (except Brazil)` 755
- `spanish_hispanic_origin.Spanish surname only` 756
- `spanish_hispanic_origin.Spanish, NOS; Hispanic, NOS; Latino, NOS` 757
- `spanish_hispanic_origin.Uknown whether Spanish/Hispanic or not` 758
- `year_of_birth` 759
- `year_of_diagnosis` 760
- `month` 761

and `newtarget` is the target variable, indicating whether or not the subject died in month given by the value of the `month` variable. 763

Lung Cancer Feature Selection 765

The feature set used as input into both the Random Forest and Neural Network models, after the transformation described in section Transformation of Censored Data for Machine Learning is given below and also available in full detail in the file `NewPatientLungML.html` . 766

- `cs_tumor_size` 770
- `elevation` 771
- `grade_cell type not determined` 772
- `grade_moderately differentiated` 773
- `grade_poorly differentiated` 774
- `grade_undifferentiated; anaplastic` 775
- `grade_well differentiated` 776
- `histology_recode_broad_groupings_acinar cell neoplasms` 777
- `histology_recode_broad_groupings_adenomas and adenocarcinomas` 778
- `histology_recode_broad_groupings_blood vessel tumors` 779

• histology_recode_broad_groupings_complex epithelial neoplasms	780
• histology_recode_broad_groupings_complex mixed and stromal neoplasms	781
• histology_recode_broad_groupings_cystic, mucinous and serous neoplasms	782
• histology_recode_broad_groupings_ductal and lobular neoplasms	783
• histology_recode_broad_groupings_epithelial neoplasms, NOS	784
• histology_recode_broad_groupings_fibroepithelial neoplasms	785
• histology_recode_broad_groupings_fibromatous neoplasms	786
• histology_recode_broad_groupings_germ cell neoplasms	787
• histology_recode_broad_groupings_gliomas	788
• histology_recode_broad_groupings_granular cell tumors & alveolar soft part sarcomas	789
• histology_recode_broad_groupings_lipomatous neoplasms	790
• histology_recode_broad_groupings_lipomatous neoplasms	791
• histology_recode_broad_groupings_miscellaneous bone tumors	792
• histology_recode_broad_groupings_miscellaneous tumors	793
• histology_recode_broad_groupings_mucoepidermoid neoplasms	794
• histology_recode_broad_groupings_myomatous neoplasms	795
• histology_recode_broad_groupings_myxomatous neoplasms	796
• histology_recode_broad_groupings_nerve sheath tumors	797
• histology_recode_broad_groupings_neuroepitheliomatous neoplasms	798
• histology_recode_broad_groupings_nevi and melanomas	799
• histology_recode_broad_groupings_osseous and chondromatous neoplasms	800
• histology_recode_broad_groupings_paragangliomas and glomus tumors	801
• histology_recode_broad_groupings_soft tissue tumors and sarcomas, NOS	802
• histology_recode_broad_groupings_squamous cell neoplasms	803
• histology_recode_broad_groupings_synovial-like neoplasms	804
• histology_recode_broad_groupings_thymic epithelial neoplasms	805
• histology_recode_broad_groupings_transistional cell papillomas and carcinomas	806
• histology_recode_broad_groupings_trophoblastic neoplasms	807
• histology_recode_broad_groupings_unspecified neoplasms	808
• lat	809
• laterality_Bilateral involvement, lateral origin unknown; stated to be single primary	810
• laterality_Left: origin of primary	811
• laterality_Not a paired site	812
• laterality_Only one side involved, right or left origin unspecified	813
• laterality_Paired site, but no information concerning laterality; midline tumor	814
• laterality_Right: origin of primary	815
• lng	816
• lng	817
• marital_status_at_dx_Divorced	818
• marital_status_at_dx_Married (including common law)	819
• marital_status_at_dx_Separated	820
• marital_status_at_dx_Single (never married)	821
• marital_status_at_dx_Unknown	822
• marital_status_at_dx_Unmarried or domestic partner	823
• marital_status_at_dx_Widowed	824
• month_of_diagnosis_Apr	825
• month_of_diagnosis_Aug	826
• month_of_diagnosis_Dec	827
• month_of_diagnosis_Feb	828
• month_of_diagnosis_Jan	829
• month_of_diagnosis_Jul	830
• month_of_diagnosis_Jun	831

- month_of_diagnosis_Mar 832
- month_of_diagnosis_May 833
- month_of_diagnosis_Nov 834
- month_of_diagnosis_Oct 835
- month_of_diagnosis_Sep 836
- number_of primaries 837
- race_ethnicity_Amerian Indian, Aleutian, Alaskan Native or Eskimo 838
- race_ethnicity_Asian Indian 839
- race_ethnicity_Asian Indian or Pakistani 840
- race_ethnicity_Black 841
- race_ethnicity_Chamorroan 842
- race_ethnicity_Chinese 843
- race_ethnicity_Fiji Islander 844
- race_ethnicity_Filipino 845
- race_ethnicity_Guamanian 846
- race_ethnicity_Hawaiian 847
- race_ethnicity_Hmong 848
- race_ethnicity_Japanese 849
- race_ethnicity_Kampuchean 850
- race_ethnicity_Korean 851
- race_ethnicity_Laotian 852
- race_ethnicity_Melanesian 853
- race_ethnicity_Micronesian 854
- race_ethnicity_New Guinean 855
- race_ethnicity_Other 856
- race_ethnicity_Other Asian 857
- race_ethnicity_Pacific Islander 858
- race_ethnicity_Pakistani 859
- race_ethnicity_Polynesian 860
- race_ethnicity_Samoan 861
- race_ethnicity_Thai 862
- race_ethnicity_Tongan 863
- race_ethnicity_Unknown 864
- race_ethnicity_Vietnamese 865
- race_ethnicity_White 866
- seer_historic_stage_a_Distant 867
- seer_historic_stage_a_In situ 868
- seer_historic_stage_a_Localized 869
- seer_historic_stage_a_Regional 870
- seer_historic_stage_a_Unstaged 871
- sex_Female 872
- spanish_hispanic_origin_Cuban 873
- spanish_hispanic_origin_Dominican Republic 874
- spanish_hispanic_origin_Mexican 875
- spanish_hispanic_origin_Non-Spanish/Non-hispanic 876
- spanish_hispanic_origin_Other specified Spanish/Hispanic origin (excludes Dominican Repuclic) 877
- spanish_hispanic_origin_Puerto Rican 878
- spanish_hispanic_origin_South or Central American (except Brazil) 879
- spanish_hispanic_origin_Spanish surname only 880
- spanish_hispanic_origin_Spanish, NOS; Hispanic, NOS; Latino, NOS 881
- spanish_hispanic_origin_Unknown whether Spanish/Hispanic or not 882

- year_of_birth
- year_of_diagnosis
- month

Breast Cancer Feature Selection

The feature set used as input into both the Random Forest and Neural Network models, after the transformation described in section Transformation of Censored Data for Machine Learning is given below and also available in full detail in the file `NewPatientBreastML.html`.

- cs_tumor_size
- elevation
- grade_moderately differentiated
- grade_poorly differentiated
- grade_ndifferentiated; anaplastic
- grade_well differentiated
- histology_recode_broad_groupings_adenomas and adenocarcinomas
- histology_recode_broad_groupings_adnexal and skin appendage neoplasms
- histology_recode_broad_groupings_basal cell neoplasms
- histology_recode_broad_groupings_complex epithelial neoplasms
- histology_recode_broad_groupings_cystic, mucinous and serous neoplasms
- histology_recode_broad_groupings_ductal and lobular neoplasms
- histology_recode_broad_groupings_epithelial neoplasms, NOS
- histology_recode_broad_groupings_nerve sheath tumors
- histology_recode_broad_groupings_unspecified neoplasms
- lat
- laterality_Bilateral involvement, lateral origin unknown; stated to be single primary
- laterality_Paired site, but no information concerning laterality; midline tumor
- laterality_Right: origin of primary
- lng
- marital_stats_at_dx_Divorced
- marital_stats_at_dx_Married (including common law)
- marital_stats_at_dx_Separated
- marital_stats_at_dx_Single (never married)
- marital_stats_at_dx_Unknown
- marital_stats_at_dx_Unmarried or domestic partner
- marital_stats_at_dx_Widowed
- month_of_diagnosis_Apr
- month_of_diagnosis_Aug
- month_of_diagnosis_Dec
- month_of_diagnosis_Feb
- month_of_diagnosis_Jan
- month_of_diagnosis_Jul
- month_of_diagnosis_Jun
- month_of_diagnosis_Mar
- month_of_diagnosis_May
- month_of_diagnosis_Nov
- month_of_diagnosis_Oct
- month_of_diagnosis_Sep
- race_ethnicity_Amerian Indian, Aletian, Alaskan Native or Eskimo
- race_ethnicity_Asian Indian

- race_ethnicity_Black 934
- race_ethnicity_Chinese 935
- race_ethnicity_Japanese 936
- race_ethnicity_Melanesian 937
- race_ethnicity_Other 938
- race_ethnicity_Other Asian 939
- race_ethnicity_Pacific Islander 940
- race_ethnicity_Thai 941
- race_ethnicity_Unknown 942
- race_ethnicity_Vietnamese 943
- race_ethnicity_White 944
- seer_historic_stage_a_Distant 945
- seer_historic_stage_a_In sit 946
- seer_historic_stage_a_Localized 947
- seer_historic_stage_a_Unstaged 948
- sex_Female 949
- spanish_hispanic_origin_Cuban 950
- spanish_hispanic_origin_Mexican 951
- spanish_hispanic_origin_Non-Spanish/Non-hispanic 952
- spanish_hispanic_origin_Other specified Spanish/Hispanic origin (excldes 953
Dominican Republic) 954
- spanish_hispanic_origin_Spanish surname only 955
- spanish_hispanic_origin_Spanish, NOS; Hispanic, NOS; Latino, NOS 956
- year_of_birth 957
- year_of_diagnosis 958
- month 959

and `newtarget` is the target variable, indicating whether or not the subject died in 960
month given by the value of the `month` variable. 961

and `newtarget` is the target variable, indicating whether or not the subject died in 962
month given by the value of the `month` variable. 963

Pseudocode for the Data Transformation 964

```
def train(X, T, D) 965
    // X, T, D are the original dataset 966
    X' = [] 967
    D' = [] 968

    // the transformation 969
    for each index i in X: 970
        for t=1 to T[i]: 971
            new_D = (0 if t < T[i], else D[i]) 972
            append new_D to D' 973
            new_X = (X[i], t) 974
            append new_X to X' 975

    return a decision tree trained on (X', D') 976

def pmf(h, X) 977
    // X is a single datapoint 978
    // returns an array A where A[i] = P(Y = i | X) 979
    980
    981
    982
```

```

A = []
p_so_far = 1 // this is p(T >= t | X)
for t = 1 to (the last month where h has any data):
    // h knows p(T = t | T >= t, X), we call this p_cur
    p_cur = h's prediction for (X, t)
    append (p_so_far * p_cur) to A
    p_so_far *= (1 - p_cur)

```

Breast Random Forest Model Hyperparameters

```

f = RandomForestClassifier(n_estimators=20,min_samples_split=3,
                           max_depth = 15,
                           max_features = .8,
                           n_jobs=5,verbose=2,random_state=33)

```

Colon Random Forest Model Hyperparameters

```

rf = RandomForestClassifier(n_estimators=25,min_samples_split=3,
                           max_depth = 10,
                           max_features = .5,
                           n_jobs=5,verbose=2,random_state=3)

```

Lung Random Forest Model Hyperparameters

```

rf = RandomForestClassifier(n_estimators=25,min_samples_split=3,
                           max_depth = 11,
                           max_features = .8,
                           n_jobs=5,verbose=2,random_state=3)

```

Breast Neural Network Model Architecture

The architecture of the Keras multilayer perceptron neural network model trained on the breast cancer data is given explicitly below:

```

modelbreast = Sequential()
modelbreast.add(Dense(114, input_shape=(66,) ,init='normal'))
modelbreast.add(Activation('relu'))
modelbreast.add(Dropout(0.05))
modelbreast.add(Dense(50, init='normal'))
modelbreast.add(Activation('relu'))
modelbreast.add(Dropout(0.05))

modelbreast.add(Dense(36, init='normal'))
modelbreast.add(Activation('relu'))
modelbreast.add(Dropout(0.05))

modelbreast.add(Dense(2, init='normal'))
modelbreast.add(Activation('softmax'))

rms = RMSprop(lr=0.001)

modelbreast.compile(loss='binary_crossentropy',

```



```
optimizer=rms, class_mode="binary")
```

and trained with a batch size of 1500 for 200 epochs.

Colon Cancer Neural Network Model Architecture

The architecture of the Keras multilayer perceptron neural network model trained on the colon cancer data is given explicitly below:

```
modelcolon = Sequential()
modelcolon.add(Dense(114, input_shape=(102,) ,init='normal'))
modelcolon.add(Activation('relu'))
modelcolon.add(Dropout(0.05))
modelcolon.add(Dense(50, init='normal'))
modelcolon.add(Activation('relu'))
modelcolon.add(Dropout(0.05))
```

```
modelcolon.add(Dense(35, init='normal'))
modelcolon.add(Activation('relu'))
modelcolon.add(Dropout(0.05))
```

```
modelcolon.add(Dense(2, init='normal'))
modelcolon.add(Activation('softmax'))
```

```
rms = RMSprop(lr=0.001)
```

```
modelcolon.compile(loss='binary_crossentropy',
optimizer=rms, class_mode="binary")
```

and trained with a batch size of 1500 for 200 epochs.

Lung Cancer Neural Network Model Architecture

The architecture of the Keras multilayer perceptron neural network model trained on the lung cancer data is given explicitly below:

```
modellung = Sequential()
modellung.add(Dense(114, input_shape=(114,) ,init='normal'))
modellung.add(Activation('relu'))
modellung.add(Dropout(0.1))
modellung.add(Dense(80, init='normal'))
modellung.add(Activation('relu'))
modellung.add(Dropout(0.1))
modellung.add(Dense(40, init='normal'))
modellung.add(Activation('relu'))
modellung.add(Dropout(0.1))
```

```

modellung.add(Dense(2, init='normal'))
modellung.add(Activation('softmax'))

rms = RMSprop(lr=0.001)

modellung.compile(loss='binary_crossentropy',
                  optimizer=rms, class_mode="binary")

and trained with a batch size of 2000 for 50 epochs.

```

S1 Video

Bold the first sentence. Maecenas convallis mauris sit amet sem ultrices gravida. Etiam eget sapien nibh. Sed ac ipsum eget enim egestas ullamcorper nec euismod ligula. Curabitur fringilla pulvinar lectus consectetur pellentesque.

S1 Text

Lorem Ipsum. Maecenas convallis mauris sit amet sem ultrices gravida. Etiam eget sapien nibh. Sed ac ipsum eget enim egestas ullamcorper nec euismod ligula. Curabitur fringilla pulvinar lectus consectetur pellentesque.

S1 Fig

Lorem Ipsum. Maecenas convallis mauris sit amet sem ultrices gravida. Etiam eget sapien nibh. Sed ac ipsum eget enim egestas ullamcorper nec euismod ligula. Curabitur fringilla pulvinar lectus consectetur pellentesque.

S2 Fig

Lorem Ipsum. Maecenas convallis mauris sit amet sem ultrices gravida. Etiam eget sapien nibh. Sed ac ipsum eget enim egestas ullamcorper nec euismod ligula. Curabitur fringilla pulvinar lectus consectetur pellentesque.

S1 Table

Lorem Ipsum. Maecenas convallis mauris sit amet sem ultrices gravida. Etiam eget sapien nibh. Sed ac ipsum eget enim egestas ullamcorper nec euismod ligula. Curabitur fringilla pulvinar lectus consectetur pellentesque.

Acknowledgments

Cras egestas velit mauris, eu mollis turpis pellentesque sit amet. Interdum et malesuada fames ac ante ipsum primis in faucibus. Nam id pretium nisi. Sed ac quam id nisi malesuada congue. Sed interdum aliquet augue, at pellentesque quam rhoncus vitae.

References

1. Sebastian Raschka. Python Machine Learning Essentials. Packt Publishing; 2015.

2. Cam Davidson-Pilon. Quickstart – lifelines 0.8.0.1 documentation; 2016 (accessed 14 Jan 2016).
<http://lifelines.readthedocs.org/en/latest/Quickstart.html>.
3. Van Poucke S, Zhang Z, Schmitz M, Vukicevic M, Laenen MV, Celi LA, et al. Scalable predictive analysis in critically ill patients using a visual open data analysis platform. PLoS ONE. 2016;11(1). Cited By 0. Available from:
<http://www.scopus.com/inward/record.url?eid=2-s2.0-84953931466&partnerID=40&md5=7a0cad7137c03146e4b75f3295f84cc6>.
4. National Cancer Institute, the Surveillance, Epidemiology, and End Results Program. About the SEER Program - SEER; 2016 (accessed 14 Jan 2016).
<http://seer.cancer.gov/about>.
5. Shin, Hyunjung and Nam, Yonghyun; ISCB Asia. A coupling approach of a predictor and a descriptor for breast cancer prognosis [Article; Proceedings Paper]. BMC MEDICAL GENOMICS. 2014 MAY 8;7(1). 3rd Annual Translational Bioinformatics Conference (TBC) / ISCB-Asia, Seoul, SOUTH KOREA, OCT 02-04, 2013.
6. Zolbanin, Hamed Majidi and Delen, Dursun and Zadeh, Amir Hassan. Predicting overall survivability in comorbidity of cancers: A data mining approach [Article]. DECISION SUPPORT SYSTEMS. 2015 JUN;74:150–161.
7. Gordon L, Olshen RA. Tree-structured survival analysis. Cancer Treatment Reports. 1985;69(10):1065–1068. Cited By 97. Available from:
<http://www.scopus.com/inward/record.url?eid=2-s2.0-0021875130&partnerID=40&md5=9e112ed840960f801b6260b23bf6811d>.
8. Bou-Hamad I, Larocque D, Ben-Ameur H. A review of survival trees. Statistics Surveys. 2011;5:44–71. Cited By 15. Available from:
<http://www.scopus.com/inward/record.url?eid=2-s2.0-84857308440&partnerID=40&md5=f8af82017ade68e335fd258c6857bf49>.
9. Ishwaran H, Kogalur UB. Consistency of random survival forests. Statistics and Probability Letters. 2010;80(13-14):1056–1064. Cited By 26. Available from:
<http://www.scopus.com/inward/record.url?eid=2-s2.0-77953020220&partnerID=40&md5=1e4478c51150f0159fdc6c1cb631968b>.
10. National Cancer Institute, the Surveillance, Epidemiology, and End Results Program. Documentation for ASCII Text Data Files - SEER Datasets; 2016 (accessed 15 Jan 2016). <http://seer.cancer.gov/data/documentation.html>.
11. Michael Bowles. Machine Learning in Python: Essential Techniques for Predictive Analysis. Wiley; 2015.
12. Allen Downey. Think Stats. O'Reilly Media; 2014.
13. United States Census Bureau. 2010 FIPS Code Files for Counties - Geography - U.S. Census Bureau; 2016 (accessed 18 Jan 2016).
<https://www.census.gov/geo/reference/codes/cou.html>.
14. Google Developers. The Google Maps Geocoding API — Google Maps Geocoding API — Google Developers; 2016 (accessed 18 Jan 2016).
<https://developers.google.com/maps/documentation/geocoding/intro>.

15. Google Developers. The Google Maps Elevation API — Google Maps Elevation API — Google Developers; 2016 (accessed 18 Jan 2016). <https://developers.google.com/maps/documentation/elevation/intro?hl=en>.
16. IOBS. Supplemental Material — PAPERDATA; 2016 (accessed 18 Jan 2016). <https://github.com/doolingdavid/PAPERDATA.git>.
17. Kaplan EL, Meier P. Nonparametric Estimation from Incomplete Observations. *Journal of the American Statistical Association*. 1958;53(282):457–481. Cited By 34216. Available from: <http://www.scopus.com/inward/record.url?eid=2-s2.0-33845382806&partnerID=40&md5=1b3d05fab93fcd0e37f176c799b3cff6>.
18. Ben Kuhn. Decision trees for survival analysis; 2016 (accessed 14 Jan 2016). <http://www.benkuhn.net/survival-trees>.
19. James Surowiecki. *The Wisdom of Crowds*. Doubleday; 2004.
20. John Cassidy. What killed Intrade?; 13 Mar 2013 (accessed 25 Jan 2016). <http://www.newyorker.com/news/john-cassidy/what-killed-intrade>.
21. Malcolm Gladwell. *Outliers*. Back Bay Books; 2011.
22. scikit-learn developers. 3.2.4.3.1. `sklearn.ensemble.RandomForestClassifier`; 2014 (accessed 25 Jan 2016). <http://scikit-learn.org/stable/modules/generated/sklearn.ensemble.RandomForestClassifier.html>.
23. Kaggle Inc . Random Forests — Kaggle; 2015 (accessed 25 Jan 2016). <https://www.kaggle.com/wiki/RandomForests>.
24. Michael Nielsen. *Neural Networks and Deep Learning*; Jan 2016 (accessed 25 Jan 2016). <http://neuralnetworksanddeeplearning.com/>.
25. T Unterthiner, A Mayr, G Klambauer, and S Hochreiter. Toxicity Prediction using deep learning; 4 Mar 2015 (accessed 25 Jan 2016). <http://arxiv.org/abs/1503.01445>.
26. F Chollet. *Keras Documentation*; 2015 (accessed 25 Jan 2016). <http://keras.io/>.